Small, highly oriented Ru grains in intermediate layer realized through suppressing relaxation of low-angle grain boundaries for perpendicular recording media

著者	Itagaki Norikazu, Saito Shin, Takahashi Migaku
journal or publication title	Journal of Applied Physics
volume	105
number	7
page range	07B734
year	2009
URL	http://hdl.handle.net/10097/51975

doi: 10.1063/1.3073947

Small, highly oriented Ru grains in intermediate layer realized through suppressing relaxation of low-angle grain boundaries for perpendicular recording media

Norikazu Itagaki,[a] Shin Saito,[b] and Migaku Takahashi[c]
Department of Electronic Engineering, Tohoku University, 6-6-05, Aoba, Aramaki, Sendai 980-8579, Japan

(Presented 13 November 2008; received 22 September 2008; accepted 7 December 2008; published online 26 March 2009)

Through analyzing the growth mechanism of the Ru layer in a nonmagnetic intermediate layer (NMIL) for perpendicular magnetic recording media, a concept for the NMIL is proposed in order to realize a recording layer of small, highly *c*-plane oriented grains with no intergranular exchange coupling. It was found that (1) fast Fourier transform analysis of plan-view transmission electron microscopy lattice images of Ru layers revealed that hexagonal close packed Ru grains in a *c*-plane oriented film readily coalesce with each other due to the disappearance of low-angle tilt boundaries. (2) A promising candidate for a NMIL consists of three individual epitaxially grown functional layers: a large-grain seed layer with a highly oriented sheet texture, a first interlayer of small grains, and a second interlayer of nonmagnetic grains isolated by a segregated oxide. (3) The $Ru-SiO_2/Ru/Mg$ NMIL based on the proposed concept exhibited small (diameter: 4.8 nm) Ru grains while retaining a narrow orientation distribution of 4.1°. © *2009 American Institute of Physics*. [DOI: 10.1063/1.3073947]

I. INTRODUCTION

To achieve perpendicular magnetic recording media with high storage densities, the recording layer (RL) grains must have a small diameter, a low-angle distribution of the magnetic easy axis, and no intergranular exchange coupling.[1] Currently used perpendicular media consist of three organized layers with different functions: a RL, a nonmagnetic intermediate layer (NMIL), and a soft magnetic underlayer (SUL). A granular layer is generally used as the RL, consisting of magnetic grains of Co-based alloy surrounded by oxide-rich boundaries.[2,3] The structural and magnetic properties of the RL are largely affected by the NMIL. Stacked layers, a crystalline seed layer (SL) and a hexagonal close packed (hcp) Ru interlayer (IL) epitaxially grown on the SL, are utilized in the NMIL for *c*-plane orientation of the Co-based crystal grains in the RL. In order to reduce the intergranular exchange coupling due to segregation of Co-based grains and SiO_2 boundaries, a Ru IL is sputtered with high-pressure Ar gas, resulting in a convex surface. However, isolation of the Co-based grains is insufficient; in the initial part of the RL, Co-based grains physically connect each other at valleys of Ru IL,[4,5] or partially cluster due to locally narrowed SiO_2 boundaries.[6] Therefore, in this paper, through analysis of the growth mechanism of the Ru layer, we propose a concept for a NMIL consisting of individual functional layers, which exhibit a RL of small and highly *c*-plane oriented grains with no intergranular exchange coupling. Furthermore, we report the successful preparation of 4.8-nm-diameter Ru grains in the NMIL.

[a]Electronic mail: norry@ecei.tohoku.ac.jp.
[b]Electronic mail: ssaito@ecei.tohoku.ac.jp.
[c]Also at New Industry Creation Hatchery Center, Tohoku University, 6-6-10, Aoba, Aramaki, Sendai 980-8579, Japan.

II. EXPERIMENTAL PROCEDURE

All samples were fabricated by direct-current magnetron sputtering onto glass substrates. The orientation and size of the crystal grains were examined by x-ray diffractometry (XRD). Specifically, orientation distributions were determined from the full width at half maximum (FWHM) of XRD rocking curves of the out-of-plane profiles. The grain diameter of each layer was estimated from the FWHM of the in-plane XRD profile using Scherrer's equation. The plane azimuth and the size distribution of the crystalline microstructure were examined by transmission electron microscopy (TEM). Plane azimuths of hcp Ru grains were analyzed via fast Fourier transform mapping (FFTM).[7] The procedure of FFTM involves (1) Fourier-transforming a 256 pixels $\times 256$ pixels (corresponding to $4.06 \times 4.06\ nm^2$) square in a high-resolution TEM image with lattice fringe originating

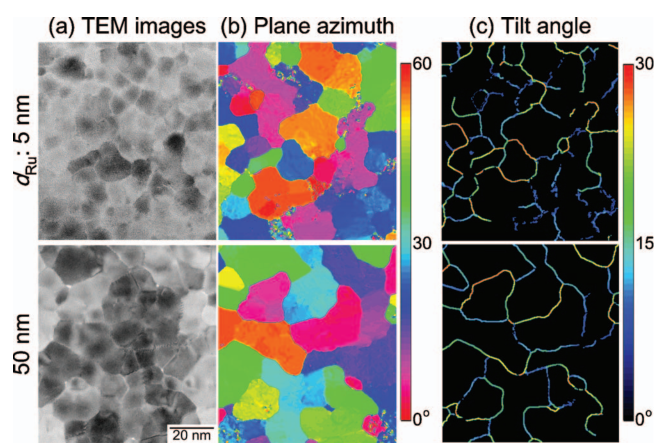

FIG. 1. (Color) (a) Plan-view bright-field images obtained by TEM, (b) images of plane azimuth of hcp(10.0), and (c) images of the tilt angle of azimuths between adjacent regions for samples with stacking structures of $/Ru(d_{Ru}\ nm)/Ni_{90}W_{10}(10\ nm)/(Fe_{65}Co_{35})_{88}B_{12}(10\ nm)/sub$. The top and bottom images correspond to samples with $d_{Ru}=5$ and 50 nm, respectively.

0021-8979/2009/105(7)/07B734/3/$25.00

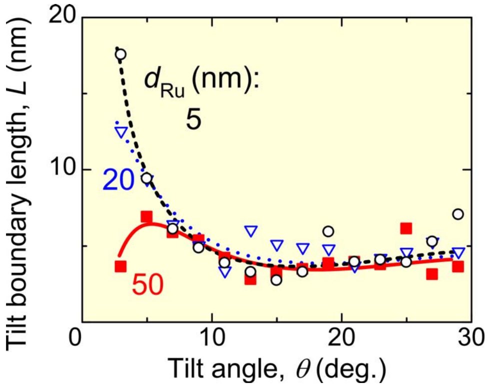

FIG. 2. (Color online) The dependence of tilt boundary length (L) per 100×100 nm^2 square on tilt angle (θ). The dashed, dotted, and solid lines correspond to the samples of d_{Ru}=5, 20, and 50 nm, respectively.

from hcp(10.0), (2) extracting a value for the plane azimuth of the strongest frequency component in the square, (3) coloring the square based on the value of plane azimuth, and (4) shifting the square by 16 pixels (0.25 nm) and repeating from step 1. Here, plane azimuth ranges cyclically from 0° to 60° due to sixfold symmetry of the c-plane. Tilt angles of the azimuth between adjacent regions in hcp Ru grains (θ) are evaluated as the difference between the plane azimuths of the regions. Here, the maximum tilt angles are 30° due to sixfold symmetry of the c-plane.

III. RESULTS AND DISCUSSION

A. Growth mechanism of *c*-plane oriented Ru

Figure 1 shows (a) a plan-view bright-field image obtained by TEM, (b) images of plane azimuth of hcp(10.0), and (c) images of the tilt angle of azimuths between adjacent regions for samples with stacking structures of Ru(d_{Ru} nm)/$Ni_{90}W_{10}$(10 nm)/$(Fe_{65}Co_{35})_{88}B_{12}$(10 nm)/sub. The images in Figs. 1(b) and 1(c) were obtained by analysis of the image in Fig. 1(a). The top and bottom images correspond to samples with d_{Ru}=5 and 50 nm, respectively. In the image in Fig. 1(b), areas with the same azimuth grow larger with increasing d_{Ru} from 5 to 50 nm. This increase indicates that grains coalesce with progressive Ru deposition. In order to clarify the mechanism of coalescence, quantitative evaluation of tilt boundaries was performed. Figure 2 shows the dependence of tilt boundary length (L) per 100×100 nm^2 square on θ for the samples of d_{Ru}=5, 20, and 50 nm. L is evaluated from the images of Fig. 1(c). In the case of d_{Ru} =5 nm, L increases with decreasing θ. Focusing on the range of $\theta<6°$, we see that L decreases with increasing d_{Ru}. This tendency suggests that the coalescence of crystal grains is caused by the disappearance of low-angle tilt boundaries. Figure 3 shows (a) a high-resolution TEM image of Ru grains with a low-angle tilt boundary of 3° and (b) a close-up of the tilt boundary. In Fig. 3(a), a disarray of contrast is observed around the low-angle tilt boundary. Figure 3(b) shows that some edge dislocations exist at the low-angle tilt boundary. Based on these results, a schematic model of the growth mechanism of Ru is shown in Fig. 4. The top schemata are plan views of the Ru surfaces, and the bottom schemata are cross sections of the Ru/seed. Here, stripes in the grains represent c-plane in plan views, and hcp(10.0) plane in cross sections, respectively. The dashed lines indicate low-angle tilt boundaries. At first, Ru islands grow on SL grains individually. Then, as Ru deposition progresses, azimuths in adjacent grains gradually align in the same direction, in order to relax the distortion energy of edge dislocations at the low-angle tilt boundaries. Thus, the coalescence causes valleys to disappear at the boundaries of Ru IL [see Fig. 4(a)], resulting in clustering of RL grains. The coalescence is easily expected to occur in films of not just Ru but other materials with an orientation plane of high crystallographic symmetry such as hcp(00.2) or face centered cubic(111).

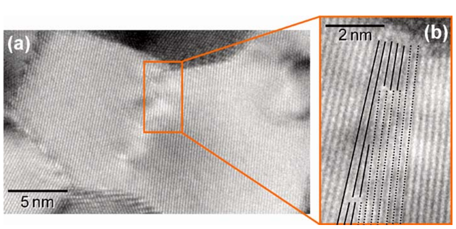

FIG. 3. (Color online) (a) A high-resolution TEM image of Ru grains with a low-angle tilt boundary of 3° and (b) a close-up of the tilt boundary. The solid and dashed lines represent hcp(10.0) planes near the boundary having a tilt angle of 3° between each other.

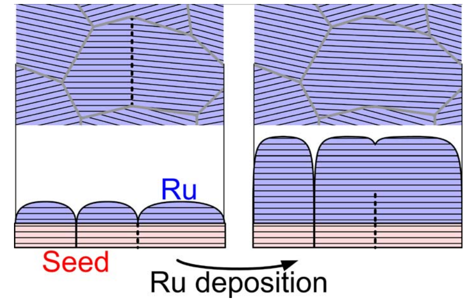

FIG. 4. (Color online) A schematic model of the growth mechanism of Ru. the top graphics are plan views of the Ru surfaces and the bottom graphics are cross sections of the Ru/seed. Stripes in grains represent c-plane in plan views and hcp(10.0) plane in cross sections, respectively. The dashed lines mean low-angle tilt boundaries.

B. Concept of a nonmagnetic intermediate layer

Figure 5 shows a schematic for the deposition process of the new concept NMIL. The NMIL consists of three individual epitaxially grown functional layers: a SL with a highly oriented sheet texture, a first IL (IL1) of small grains, and a

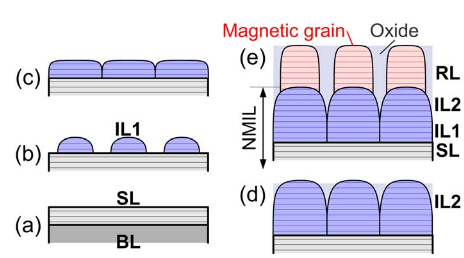

FIG. 5. (Color online) A schematic for the deposition process of the NMIL to realize a RL with small, highly c-plane oriented and magnetically isolated grains. Each diagram represents growth of (a) a SL on a BL, [(b) and (c)] a first interlayer (IL1), (d) a second interlayer (IL2), and (e) a RL.

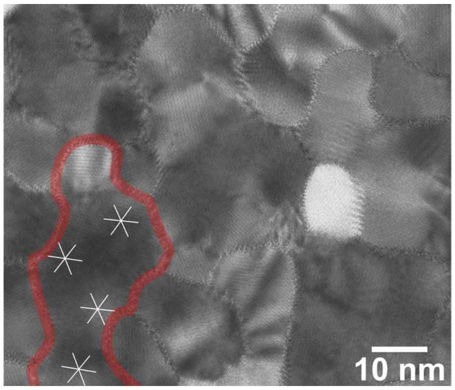

FIG. 6. (Color online) A plan-view TEM image for a sample with stacking structure of Ru (20 nm)/Mg (20 nm)/NiFeCr (20 nm)/sub. The thick lines and star marks represent typical examples of the boundaries with moiré pattern and plane azimuths of hcp(10.0), respectively.

second IL (IL2) of segregated grains. In stage (a), a SL of large grains leads to highly oriented sheet texture. Large grains are obtained by a Frank–van der Merwe growth mode (layer-by-layer growth). Hence, materials with low surface energies are suitable for the SL.[8] In stages (b) and (c), dense initial islands on the SL grow into small grains. IL1, with a high nucleation density, is induced by the Volmer–Weber growth mode (island growth). Thus, required properties of the IL1 are a low wettability and a large lattice misfit against the SL.[9] In stage (d), oxide segregation prevents IL2 grains from coalescing and retains small grains. Finally, in stage (e), the Co-based grains of the RL are individually grown on the IL grains. Furthermore, oxide boundaries of IL2 suppress intergranular exchange coupling at the initial part of the granular RL. Therefore, the material for each layer must be selected by considering the epitaxial growth mode.

C. Proposal of Ru–SiO_2/Ru/Mg NMIL

In order to realize the NMIL of the proposed concept, Mg was selected as a SL material because it is a hcp metal with a large misfit against Ru and a low surface energy.[9] To investigate stages (b) and (c) of Fig. 5, a plan-view TEM image was observed for a sample with stacking structure of Ru (20 nm)/Mg (20 nm)/NiFeCr (20 nm)/sub (Fig. 6). The XRD measurements revealed that grains in the Ru layer have a small diameter of 8.3 nm, whereas those in the Mg layer have a large diameter of over 15 nm.[9] Regions of irregular shapes surrounded by boundaries exhibiting a moiré pattern are observed in the TEM image (e.g., region enclosed by the thick line in Fig. 6). The size of the irregular regions is over 30 nm. Plane azimuths inside one irregular grain are almost the same. The irregular region consists of some regions that are approximately 7–10 nm in size and that exhibit variable light/dark contrast. The sizes of these regions are nearly equal to the grain diameter determined by XRD. These results signify that small Ru islands epitaxially grown on one large Mg grain readily coalesce because of the same plane azimuth of Ru islands.

Finally, the NMIL of stage (d) in Fig. 5 was investigated with stacking structure of $Ru_{93}-(SiO_2)_7$ (15 nm)/Ru (5 nm)/Mg (20 nm)/Ta (5 nm)/sub. Here, nanocrystalline Ta was selected as the material for the amorphous-like[10] buffer layer (BL), since the SUL in the actual media is amorphous. Figure 7 shows (a) a plan-view TEM image and (b) a histogram for the grain diameters of the Ru–SiO_2 layer. The Mg SL on the Ta BL also consists of large grains of over 15 nm in diameter. In the TEM image (a), the dark grains are densely packed, almost without clustering, and a bright mesh texture is observed, indicating that the Ru grains are surrounded by SiO_2-rich boundaries. The Ru grains have a small average diameter of 4.8 nm. XRD measurements revealed that Ru grains are *c*-plane oriented and have a narrow orientation distribution of 4.1°. Thus, the proposed concept was found to create small, isolated NMIL grains while retaining a narrow orientation distribution. A RL with small isolated grains can be achieved by growing a granular layer of Co-based alloy with an adequate volume ratio of SiO_2 on the proposed NMIL.

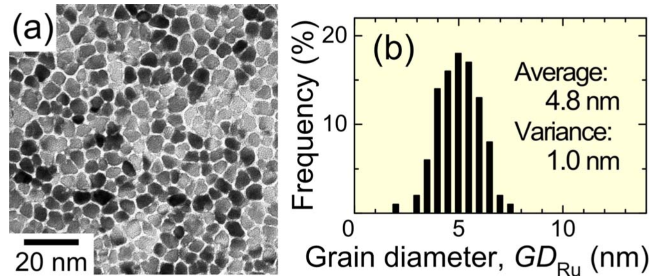

FIG. 7. (Color online) (a) A plan-view TEM image of the Ru–SiO_2 layer and (b) histogram for the grain diameters of the Ru–SiO_2 layer for a stacking structure of $Ru_{93}-(SiO_2)_7$ (15 nm)/Ru (5 nm)/Mg (20 nm)/Ta (5 nm)/sub.

ACKNOWLEDGMENTS

This study was partially supported by the Industrial Technology Research Grant Program in 2006 from NEDO of Japan. The authors would like to thank Hitachi Metals, Ltd. for providing NiW sputtering targets. The authors are deeply grateful to Mr. T. Araki, Mr. I. Shibuya, and Ms. K. Seimiya from Foundation for Promotion of Material Science and Technology of Japan for the TEM observation and the FFT.

[1]S. N. Piramanayagam, J. Appl. Phys. **102**, 011301 (2007).
[2]T. Oikawa, M. Nakamura, H. Uwazumi, T. Shimatsu, H. Muraoka, and Y. Nakamura, IEEE Trans. Magn. **38**, 1976 (2002).
[3]M. Zheng, B. R. Acharya, G. Choe, J. N. Zhou, Z. D. Yang, E. N. Abarra, and K. E. Johnson, IEEE Trans. Magn. **40**, 2498 (2004).
[4]I. Takekuma, R. Araki, M. Igarashi, H. Nemoto, I. Tamai, Y. Hirayama, and Y. Hosoe, J. Appl. Phys. **99**, 08E713 (2006).
[5]S. Saito, T. Ueno, S. Sasaki, and M. Takahashi, J. Vac. Soc. Jpn. **51**, 578 (2008).
[6]H. S. Jung, M. Kuo, S. S. Malhotra, and G. Bertero, J. Appl. Phys. **103**, 07F515 (2008).
[7]T. Ide, A. Sakai, and K. Shimizu, Jpn. J. Appl. Phys., Part 2 **37**, L1546 (1998).
[8]W. Seifert, N. Carlsson, M. Miller, M.-E. Pistol, L. Samuelson, and L. R. Wallenberg, Prog. Cryst. Growth Charact. Mater. **33**, 423 (1996).
[9]N. Itagaki, S. Saito, and M. Takahashi, J. Phys. D **41**, 152006 (2008).
[10]M. Zheng, G. Choe, K. E. Johnson, L. Gao, and S. H. Liou, IEEE Trans. Magn. **38**, 1979 (2002).